

# Staged Voxel-Level Deep Reinforcement Learning for 3D Medical Image Segmentation with Noisy Annotations

YuYang Fu<sup>1</sup>, XiuZhen Guo<sup>2</sup>, Ji Shi<sup>1\*</sup>

<sup>1\*</sup>the Academy for Multidisciplinary Studies, Beijing National Center for Applied Mathematic, Capital Normal University, Beijing, 100048, China.

<sup>1</sup>the School of Mathematical Science, Capital Normal University, Beijing, 100048, China.

<sup>2</sup>the School of Mathematical Science, Capital Normal University, Beijing, 100048, China.

\*Corresponding author(s). E-mail(s): [shiji@cnu.edu.cn](mailto:shiji@cnu.edu.cn);  
Contributing authors: [fyxyr@163.com](mailto:fyxyr@163.com); [xiuzhenguo589@gmail.com](mailto:xiuzhenguo589@gmail.com);

## Abstract

Deep learning has demonstrated remarkable success in medical image segmentation. Nowadays accurate segmentation results remains highly dependent on large-scale, high-quality annotated datasets. However, in practice, noisy annotations are quite common due to complex boundary geometry structure of organs in medical images and inter-observer variability in delineating ambiguous anatomical boundaries, which can severely constrain the performance of a segmentation model. Motivated by the fact that medical imaging annotator can correct labeling errors during segmentation based on prior knowledge, we propose an end-to-end Staged Voxel-Level Deep Reinforcement Learning (SVL-DRL) framework for robust medical image segmentation under noisy annotations. This framework employs a dynamic iterative update strategy to automatically mitigate the impact of erroneous labels without requiring manual intervention. The key advancements of SVL-DRL over existing works include: i) formulating noisy annotations as a voxel-dependent problem and addressing it through a novel staged reinforcement learning framework; ii) incorporating a voxel-level Asynchronous Advantage Actor-Critic (vA3C) module that conceptualizes each voxel as an autonomous agent, which allows each agent to dynamically refine its own state representation during training, thereby directly mitigating the influence of

erroneous labels and noise; iii) designing a novel action space for deep reinforcement learning agents, along with a composite reward function that strategically combines the Dice value and a spatial continuity metric to significantly boost segmentation accuracy. The proposed method achieves state-of-the-art performance on three public medical image datasets and a clinical adrenal gland dataset. It demonstrates consistent superiority across various experimental settings, with an average improvement of over 3% in both Dice and IoU scores.

**Keywords:** 3D medical image segmentation, Deep reinforcement learning, Learning with label noise

## 1 Introduction

Accurate segmentation of medical images plays a pivotal role in both clinical practice and scientific research[1–5]. In the past decade, with the rapid development of computing power, medical image segmentation methods based on deep learning have achieved great success[6, 7]. However, these methods rely on rich and accurate labeled data to obtain superior segmentation performance. In practice, ensuring the accuracy of annotated data remains a persistent challenge, particularly when working with private datasets where standardized quality control processes may be lacking[8, 9]. As a result, medical training datasets often contain noisy labels, which can mislead the segmentation model into learning incorrect semantic associations. This, in turn, compromises the model’s generalization capability[10, 11]. Therefore, developing robust medical image segmentation techniques that can handle noisy labeled data is crucial for model training.

A range of methodologies have been developed to learn from noisy labels, which can be broadly categorized into four types. First, methods based on the Noise Transition Matrix (NTM) model the transition probabilities between clean and noisy labels to correct the loss function[12, 13]. However, these methods often depend on an accurate NTM estimation, which becomes challenging under complex noise patterns. Second, sample selection-based approaches like Co-Teaching[14] and its variants utilize dual-network frameworks to mutually select small-loss samples, thereby filtering out noisy labels. Third, label correction and denoising strategies directly address noisy annotations; for instance, Confident Learning[15] identifies mislabeled pixels through joint distribution estimation, whereas JCAS[16] introduces a joint class-affinity loss that leverages pixel relationships and dynamic thresholding for noise reduction and class imbalance adaptation. Fourth, collaborative learning and distillation frameworks, such as Reliable Mutual Distillation[17], employ dual-model collaboration to mutually refine labels and distill knowledge, augmented by data and model enhancements. CLCL[18] employs a curriculum dynamic thresholding approach adapting to model learning progress to select clean data samples to mitigate the class imbalance issue.

Motivated by the fact that medical imaging annotator can correct labeling errors during segmentation based on prior knowledg, we designed our model to mimic this

capability. Accordingly, we propose a method capable of autonomously refining inaccuracies in training data by leveraging learned experience to produce highly accurate segmentation masks.

We propose an end-to-end staged voxel-level deep reinforcement learning (SVL-DRL) framework. This framework employs a dynamic iterative update strategy to automatically mitigate the impact of erroneous labels without requiring user intervention. It directly segments regions of interest by taking the original image and its corresponding labels as input. To effectively capture both local and global contextual information from the raw images, we employ Swin Unetr[19] as the baseline segmentation model. During the reinforcement learning phase, a pixel-level asynchronous advantage actor-critic mechanism is designed to perform asynchronous segmentation without manual intervention. Each voxel is treated as an agent, with its value representing the current state. Through policy and value updates, the state is iteratively refined, allowing the model to correct inaccuracies dynamically. This framework reformulates medical image segmentation as a dynamic decision-making process. It not only learns to accurately segment regions of interest but also develops the ability to resist learning incorrect information due to imperfect or deformed labels by adaptively modifying the image states. By leveraging the anatomical prior knowledge and the exploratory strength inherent in reinforcement learning, our approach produces segmentation results that are more clinically plausible, while training stability is ensured through multi-stage optimization.

In conclusion, the key contributions of this work are outlined as follows:

- We conducted an in-depth investigation into medical image segmentation under the challenging yet commonly overlooked condition of voxel-level label noise and proposed a novel staged voxel-level deep reinforcement learning framework, termed SVL-DRL, which autonomously mitigates the adverse effects of noisy labels on segmentation performance without requiring prior filtering or manual intervention.
- In the SVL-DRL framework, we introduce a voxel-level asynchronous advantage actor-critic (vA3C) module. Within this structure, each voxel is treated as an autonomous agent. This approach enables dynamic refinement of input states without discarding any training samples, thereby offering greater robustness against noise compared to conventional threshold-based selection methods.
- We designed a novel action space tailored for agents in Deep Reinforcement Learning and a composite reward function that integrates the Dice value with a spatial continuity metric to significantly enhance segmentation accuracy.
- The proposed method achieves state-of-the-art performance on three public medical image datasets. It demonstrates consistent superiority across various experimental settings, with an average improvement of over 3% in both Dice and IoU scores.

## 2 Related Works

In this section, we will introduce learning with noise labels, reinforcement learning frameworks, and noise types in medical image segmentation tasks related to our work.

## 2.1 Learning with Noise Labels

Learning with noise labels has attracted considerable attention owing to its ability to leverage large amounts of inexpensive and imprecise data [18, 20–22]. Methods on learning with noisy labels can be broadly categorized into the following classes:

First, methods based on the Noise Transition Matrix (NTM) correct the loss function by modeling the transition probability between clean labels and noisy labels. For instance, [12] introduced forward and backward correction methods, which utilize the NTM to adjust the cross-entropy loss, thereby enhancing the model’s robustness to noise. However, these methods rely on accurate estimation of the NTM, which may be limited in complex noise patterns.

Second, sample selection-based methods aim to identify and utilize clean samples for training. Co-Teaching [14] and its variants (e.g., Co-Teaching+) maintain two networks that mutually select small-loss samples for each other, thus filtering out noisy labels. In medical image segmentation, MTCL [23] combines the Mean Teacher framework with Confident Learning, where the teacher model generates reliable predictions to guide the training of the student model, effectively leveraging both high-quality and low-quality annotated data. Similarly, ADELE [24] adaptively corrects noisy labels based on the early-learning phenomenon, avoiding overfitting.

Third, label correction and denoising strategies directly handle noisy labels. Confident Learning [15] identifies mislabeled pixels by estimating the joint distribution and corrects them. JCAS [16] further introduces a joint class-affinity loss correction, leveraging relationships between pixels to reduce the noise rate and adapting to class imbalance through dynamic threshold adjustment. Additionally, the RSF-assisted method [25] aids label correction based on region-scalable fitting, incorporating image feature information to improve correction accuracy.

Fourth, collaborative learning and knowledge distillation frameworks are widely applied in noisy label handling. For example, Reliable Mutual Distillation [17] employs dual-model collaboration to mutually clean labels and distill reliable knowledge, combined with data and model augmentation to enhance robustness. MS-TFAL [26] utilizes temporal feature affinity learning in video sequences to supervise the model at multiple scales, reducing the impact of noise. CLCL [18] employs a curriculum dynamic thresholding approach adapting to model learning progress to select clean data samples to mitigate the class imbalance issue.

## 2.2 Deep Reinforcement Learning

Deep Reinforcement Learning (DRL) integrates deep neural networks with reinforcement learning, enabling agents to learn optimal policies directly from high-dimensional sensory inputs through environmental interaction. In the field of medical image analysis, particularly in medical image segmentation, various deep reinforcement learning algorithms have been extensively studied and successfully applied. For instance, [27] first introduces the concept of context-specific segmentation, which adapts the model to both the defined objective function and the user’s intent and prior knowledge. [28] proposes a multi-agent reinforcement learning approach incorporating user interaction, aiming to capture voxel dependencies while reducing the exploration space to a

manageable size. Additionally, [29] presents an end-to-end policy strategy based on deep reinforcement learning.

While these approaches demonstrate promise in medical image tasks, they often face challenges in training stability and computational efficiency, especially when handling complex, high-dimensional data. To address these limitations, the Asynchronous Advantage Actor-Critic (A3C)[30] method has emerged as a groundbreaking framework in deep reinforcement learning. A3C utilizes multiple actor-learners executing in parallel across multiple environment instances. Each learner asynchronously performs gradient updates to a shared global model, which decorrelates the data and mitigates non-stationarity issues inherent in online reinforcement learning. The algorithm combines an actor that updates the policy  $\pi(a|s; \theta)$  with a critic that estimates the value function  $V(s; \theta_v)$ , using  $n$ -step returns to compute the advantage function  $A(s, a)$  for policy gradient updates.

### 2.3 Noise Type for Segmentation Tasks

Most existing methods designed to handle artificially synthesized label noise were initially developed for image classification tasks[31, 32]. In such contexts, synthesized label noise typically encompasses both symmetric and asymmetric types. Symmetric label noise refers to the random flipping of true labels to any other class with equal probability, whereas asymmetric label noise involves flipping labels according to specific, structured rules. However, these synthetic noise models are often inadequate for segmentation tasks, as they do not accurately reflect the nature of real annotation errors.

In contrast to classification-oriented noise models, label noise in Source-Free Domain Adaptation (SFDA) follows a different distribution pattern[33]. SFDA noise is generated when a pre-trained model is adapted to annotate new data, often introducing systematic biases. As demonstrated in [33], conventional noisy-label learning methods—reliant on explicit noise distribution assumptions—are frequently ineffective in addressing SFDA-induced label errors. Alternatively, to better simulate human annotation mistakes in segmentation, previous works such as [34] introduced morphological transformations—such as random erosion or dilation—applied at varying ratios to simulate imperfect manual annotations.

Our work incorporates both SFDA-induced noise and morphologically transformed labels, as these represent more realistic and challenging noise profiles pertinent to image segmentation. Illustrations of the noise types employed in our study are provided in Fig. 2.

## 3 Method

In this section, we introduce our SVL-DRL framework for 3D Medical image segmentation with noisy labels in detail. We first give a brief problem statement and an overview of our method in 3.1, and then explain the two main modules of our method, i.e., staged deep reinforcement learning module and the voxel-level asynchronous advantage Actor Critic module, in 3.2 and 3.3, respectively.

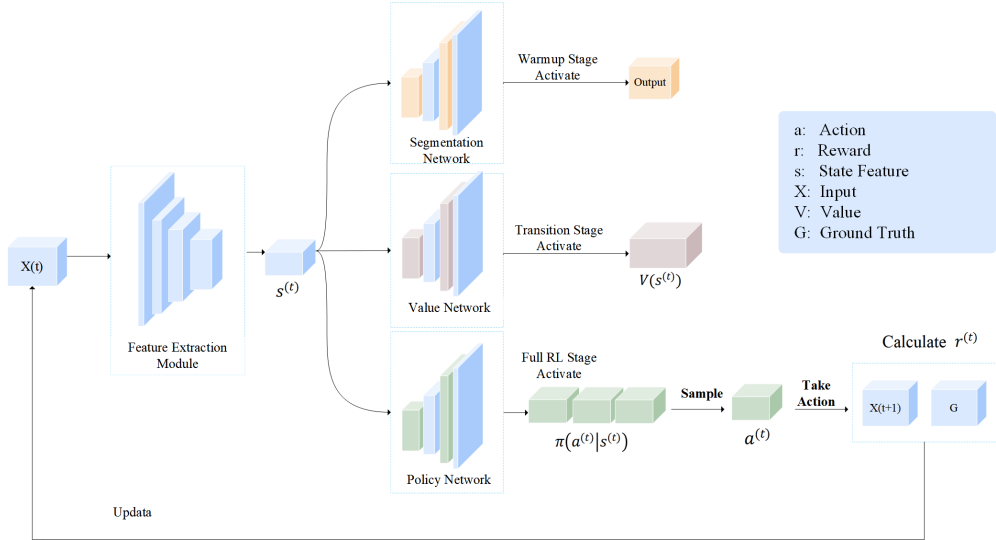


**Fig. 1** The overall framework of SVL-DRL. The SVL-DRL architecture is based on PA3C combining swin-unetr.  $X^{(t)}$  is the temporary input in step  $t$ ,  $GT$  is the label.  $a^{(t)}$  is sampled from the policy  $\pi : a^{(t)} \sim \pi(a^{(t)} | s^{(t)})$ .

### 3.1 Overview

In the context of medical image segmentation with noisy labels, we are given a set of medical images  $\mathcal{X} = \{x_i\}_{i=1}^N$  and the corresponding annotations  $\mathcal{Y} = \{y_i\}_{i=1}^N$ . The input image  $x_i \in \mathbb{R}^{H \times W \times D}$  has a spatial size of  $H \times W \times D$ , while  $y_i \in \{0, 1\}^{H \times W \times D \times C}$  is the one-hot ground truth segmentation mask, where  $C$  indicates the number of visual classes in total. Note that the annotations in the training phase are subject to noise, meaning some labels are incorrect. Besides, the identities of the correct and erroneous annotations within the training set remain unknown. In contrast, clean annotations are solely used for performance validation during the inference phase.

The overview of our proposed SVL-DRL framework is shown in fig.1. Our SVL-DRL framework consists of three stages: Warmup stage, Transition stage and Full RL stage. In Warmup stage, only the parameters of the segmentation network are activated because the neural network can prioritize learning easy to learn information, which enables the model to initially master segmentation ability. In Transition stage, the parameters of the value network are also activated and it has not progressed to the reinforcement learning stage. This stage equips the value network with state evaluation capabilities, thus facilitating action sampling in the subsequent Full RL stage. In Full RL stage, the deep reinforcement learning module is activated to correct the impact of incorrect labels on the segmentation model learning by modifying the input image state features through the pixel level asynchronous advantage Actor Critic module. The baseline segmentation model we have chosen is Swin Unetr[19], which possesses the powerful global context modeling ability of Transformer and the excellent local detail recovery and multi-scale feature fusion ability of U-Net.

### 3.2 Staged deep reinforcement learning module

As seen from fig.1, the core of our method is staged deep reinforcement learning module. It is based on a shared encoder and three independent decoders. The segmentation decoder outputs the final segmentation prediction probability map, the value decoder outputs a value prediction, and the strategy decoder outputs an action probability map.

In Warmup stage, we train the complete baseline segmentation model and use Dice loss for backpropagation. This can avoid training divergence caused by reinforcement learning components (policy networks/value networks) in random parameter states. Given predicted probability map  $P$  and ground truth  $G$ , the Warmup stage loss is defined as:

$$\mathcal{L}_{\text{Warmup stage}} = \mathcal{L}_{\text{Dice Loss}} = 1 - \text{Dice}(P, G) \quad (1)$$

In Transition stage, we introduce time difference learning to establish the ability of state value assessment. The value network utilize the current state  $s^{(t)}$  at time step  $t$ , which is the feature map containing global information, as their input. Then the value network produces the value  $V(s^{(t)})$ , which reflects the anticipated total rewards for the state  $s^{(t)}$  and provides insight into the desirability of the current state. The formula for multi-step discount return is as follows:

$$R^{(t)} = r^{(t)} + \gamma r^{(t+1)} + \gamma^2 r^{(t+2)} + \dots + \gamma^{(n)} r^{(t+n)} \quad (2)$$

Where  $\gamma$  represents the discount factor and  $r^{(t)}$  denotes the immediate reward received at time step  $t$ , the specific definition can be found in formula (11). The loss of the value network is defined as follow:

$$\mathcal{L}_{\text{value}} = (R^{(t)} - V(s^{(t)}))^2 \quad (3)$$

The Transition stage loss is defined as follows:

$$\mathcal{L}_{\text{Transition stage}} = ((1 - \lambda)\mathcal{L}_{\text{Dice Loss}} + \lambda\mathcal{L}_{\text{value}}) \quad (4)$$

Here,  $\lambda \in (0, 1)$  and is used to control the weights of the two decoders.

In Full RL stage, the policy network generates the policy  $\pi(a^{(t)}|s^{(t)})$  for selecting action  $a^{(t)} \in \delta$ . As a result, the policy network has output channels equal to  $|\delta|$ .

$$A(a^{(t)}, s^{(t)}) = R^{(t)} - V(s^{(t)}) \quad (5)$$

where  $A(a^{(t)}, s^{(t)})$  is the advantage function, which represents the advantage of taking an action in the current state relative to the average expectation, and  $V(s^{(t)})$  is subtracted to reduce the variance of the gradient.

$$\mathcal{L}_{\text{policy}} = -\log \pi(a^{(t)}|s^{(t)})A(a^{(t)}, s^{(t)}) \quad (6)$$

The Full RL stage loss is defined as follows:

$$\mathcal{L}_{\text{Full RL stage}} = (1 - \alpha - \beta)\mathcal{L}_{\text{Dice Loss}} + \alpha\mathcal{L}_{\text{value}} + \beta\mathcal{L}_{\text{policy}} \quad (7)$$

Here,  $\alpha, \beta \in (0, 1)$ ,  $(\alpha + \beta) \in (0, 1)$  are used to control the weights of the three decoders.

### 3.3 voxel-level asynchronous advantage Actor Critic module

We propose vA3C, which improves the policy and the value network, so that it can treat each voxel as an agent with an independent voxel-level behavior strategy unlike other methods that share weight strategies.

We represent the  $i$ -th voxel in the medical image  $I$  (with a total of  $N$  voxels, where  $i = 1, 2, \dots, N$ ) as  $I_i$ . Each voxel is characterized by a policy denoted as  $\pi_i(a_i^{(t)}|s_i^{(t)})$ , where  $a_i^{(t)} \in A$  and  $s_i^{(t)}$  represent the action and state of the  $i$ -th agent at time step  $t$ . Obviously,  $s_i^{(0)} = I_i$ , the agents receive subsequent states  $s^{(t+1)} = (s_1^{(t+1)}, \dots, s_N^{(t+1)})$  and rewards  $r^{(t+1)} = (r_1^{(t+1)}, \dots, r_N^{(t+1)})$  by executing actions  $a^{(t+1)} = (a_1^{(t+1)}, \dots, a_N^{(t+1)})$ . The aim of pixel-level deep reinforcement learning is to learn the optimal policies  $\pi = (\pi_1, \dots, \pi_N)$  to maximize the mean of the total expected rewards across all pixels of the medical image:

$$\pi^* = \operatorname{argmax}_{\pi} E_{\pi} \left( \sum_{t=0}^{\infty} \gamma^t \bar{r}^{(t)} \right), \quad (8)$$

$$\bar{r}^{(t)} = \frac{1}{N} \sum_{i=1}^N r_i^{(t)}, \quad (9)$$

where  $\bar{r}$  stands for the mean of the rewards  $r_i^{(t)}$ .

To prevent an excessive increase in the number of model parameters and algorithm complexity, we only design three actions, that is, set to 0 (i.e., doing nothing), 1 (i.e., enhance tissues or lesions) or 2 (i.e., weaken tissues or lesions).

$$I_{\text{new}} = \begin{cases} I_{\text{ori}}, & a^{(t)} = 0 \\ \min \left( \max (I_{\text{orig}} \times (1.0 + 0.3\epsilon), 0.0), 1.0 \right), & a^{(t)} = 1 \\ \min \left( \max (I_{\text{orig}} \times (1.0 - 0.3\epsilon), 0.0), 1.0 \right), & a^{(t)} = 2 \end{cases} \quad (10)$$

Here,  $\epsilon \sim U(0, 1)$  is a random scaling coefficient, where  $U$  denotes the uniform distribution. For clarity of representation, the three-channel action output is converted into a single-channel label.

In deep reinforcement learning, the design of the reward function is particularly crucial as it determines the specific direction for model optimization. In most tasks, the most straightforward approach is to reward the model with +1 when it performs well and -1 when its performance is poor. However, unlike game tasks, there are no direct evaluation criteria in this task. Additionally, if the reward is simply a constant, it would not be conducive to encouraging the model to make significant progress, nor would it effectively penalize severe errors. Therefore, we design the reward function such that: a positive reward is assigned when the current segmentation outperforms the previous result, while inferior performance yields a negative reward. For the reward  $r^{(t)}$  at each step  $t$ , it is calculated by:

$$r^{(t)} = \underbrace{\Delta \text{Dice}(f^{(t)}, f^{(t-1)}, G)}_{\text{segmentation improvement}} + \underbrace{\mathcal{C}(f^{(t)})}_{\text{anatomical constraint}} \quad (11)$$

where:

$$\Delta\text{Dice}(f^{(t)}, f^{(t-1)}, G) = \text{Dice}(f^{(t)}, G) - \text{Dice}(f^{(t-1)}, G) \quad (12)$$

$f^{(t)} \in [0, 1]^{H \times W \times D}$  is current step segmentation probability map;  $f^{(t-1)} \in [0, 1]^{H \times W \times D}$  is previous step segmentation probability map.

$\mathcal{C}(f)$  evaluates the anatomical plausibility of the segmentation based on organ-specific characteristics such as connectivity and smoothness for the organ. The anatomical plausibility constraint  $\mathcal{C}(f)$  is formally defined as:

$$\mathcal{C}(f) = \max(N_{\text{cc}}(f) - 1, 0) + \sum_{i,j} |\nabla f_{i,j}| \quad (13)$$

$$\sum_{i,j} |\nabla f_{i,j}| = \sum_{i,j} \sqrt{(f_{i+1,j} - f_{i,j})^2 + (f_{i,j+1} - f_{i,j})^2} \quad (14)$$

where  $N_{\text{cc}}(f)$  counts the number of connected components in the mask  $f$ .

Consequently, Algorithm 1 summarizes the training processes of the proposed Staged Voxel-level Deep Reinforcement Learning Algorithm.

## 4 Experiments

### 4.1 Implementation Details

Our method is implemented by PyTorch and trained on a single Nvidia RTX4090Ti GPU. We employ Swin-Unetr as the backbone network. The SGD optimizer is adopted. The initial learning rate is set as 1e-4. We adopt a batch size of 1 and a maximum epoch number of 1000. The loss weights  $\alpha$ ,  $\beta$  and  $\lambda$  are set to 0.2, 0.2 and 0.3 respectively, for both of the three datasets. For a fair comparison, we keep the same backbone for all baselines. For our model, we only use one branch to evaluate the model so that the model weights are at the similar level as other methods in comparison. The whole segmentation framework is trained in an end-to-end fashion. The segmentation performance was evaluated using four standard metrics: the Dice Similarity Coefficient (Dice), Intersection over Union (IoU), 95th percentile Hausdorff Distance (HD95), and Average Symmetric Surface Distance (ASD).

### 4.2 Datasets

We validate the method on the LA, Pancreas-CT, BraTS 2021 datasets.

**The LA dataset[35]:** the 2018 Atrial Segmentation Challenge 1, contains 80 gadolinium-enhanced MR imaging scans for training and 20 enhanced MR imaging scans for testing, with an isotropic resolution of  $0.625 \times 0.625 \times 0.625$  mm. we used a fixed split that 80 samples are training and the rest 20 samples are for validation. Then, we report the performance of our model and other methods on the same validation set for fair comparisons. Patches are  $96 \times 96 \times 96$ , with sliding window prediction for testing.

**The Pancreas-CT dataset[36]:** containing 82 3D abdominal contrast-enhanced CT scans, which were collected from 53 male and 27 female subjects at the National

Institutes of Health Clinical Center. These slices are collected on Philips and Siemens MDCT scanners and have a fixed resolution of  $512 \times 512$  with varying thicknesses from 1.5 to 2.5 mm. The data split is fixed in this paper as the DTC model[37]. We employed 62 samples for training and reported the performance of the rest 20 samples. We here clipped the voxel values to the range of  $[-125, 275]$  Hounsfield Units (HU) as [38] and further re-sampled the data into an isotropic resolution of  $1.0 \times 1.0 \times 1.0$  mm. Patches are  $96 \times 96 \times 96$ , with sliding window prediction for testing.

**The BraTS 2021 dataset [39]:** comprising 1,251 subjects. For each subject, four co-registered 3D MRI sequences are provided: (a) native T1-weighted (T1), (b) post-contrast T1-weighted (T1Gd), (c) T2-weighted (T2), and (d) T2 Fluid-Attenuated Inversion Recovery (FLAIR). All images have been skull-stripped, rigidly aligned, and resampled to an isotropic resolution of  $1.0 \times 1.0 \times 1.0$  mm. The image size is  $240 \times 240 \times 155$ . The annotations were combined into three nested sub-regions: Whole Tumor (WT), Tumor Core (TC), and Enhancing Tumor (ET). Our models were trained on BraTS 2021 dataset with 1000 and 251 cases in the training and validation sets, respectively. Patches are  $128 \times 128 \times 128$ , with sliding window prediction for testing.

### 4.3 Noise Patterns

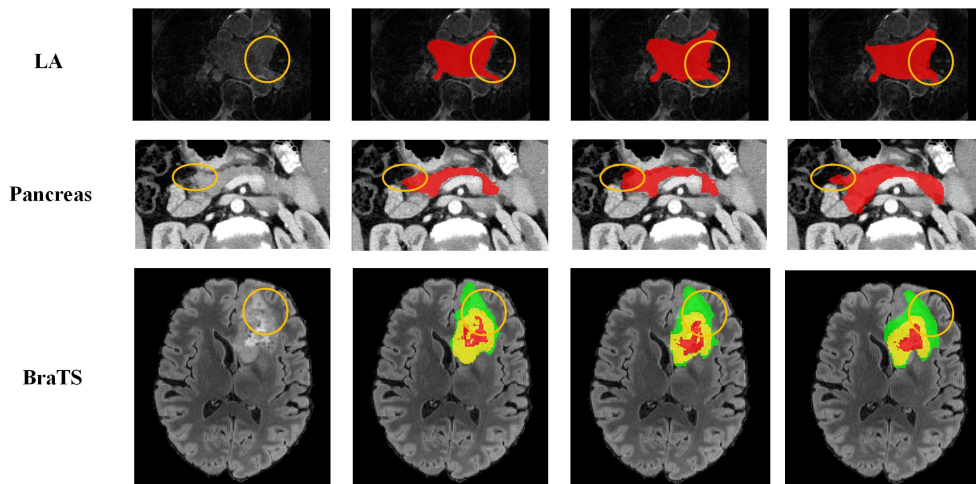


**Fig. 2** Visual comparison of different noisy labels on different datasets. Column 1: original images; Column 2: images with clean segmentation labels; Column 3: images with TC-Noise labels; Column 4: images with SFDA-Noise labels

To thoroughly evaluate the robustness of each method, we perform experiments under two types of synthetic label noise: SFDA noise[33] and morphologically transformed noise[34]. For SFDA noise, we first train a source domain model on a subset of the training data, and then use this model to predict labels for another disjoint subset, thereby generating realistic noisy annotations. For morphological noise, we simulate

annotation inaccuracies by applying morphological operations such as dilation or erosion to the ground truth labels. These synthetic noise patterns are designed to mimic real-world annotation artifacts. Example illustrations of the resulting noisy labels are provided in Fig. 2. The noise ratio of these three datasets is 50%.

#### 4.4 Methods in comparison

To evaluate the effectiveness of our proposed method under noisy label conditions, we compared it with four categories of state-of-the-art approaches: loss correction methods, sample selection-based methods, label correction and denoising strategies, and collaborative learning with knowledge distillation frameworks (Loss Correction[12], Co-Teaching[14], MTCL[23], ADELE[24], JCAS[16], RSF-assisted[25], CLCS[18]). We implemented these methods under the same 3D medical image segmentation framework and compared them using a common baseline model (Swin Unetr[19]).

#### 4.5 Performance Comparison

In this section, we evaluate the segmentation performance of different methods on three medical image datasets with different types of noise.

##### 4.5.1 Results on the LA dataset

Table 1 presents the quantitative comparison results on the LA dataset [35] with two different types of noisy labels: SFDA noise (denoted as SFDA-Noise) and morphologically transformed noise (denoted as MT-Noise). Under the typical supervised setting, the baseline network achieves poor performance on both Dice and IoU metrics when trained with noisy labels.

All label-noise robust learning methods outperform the baseline, with our proposed SVL-DRL achieving state-of-the-art results across both noise settings. Specifically, our method improves the Dice score by 5.28% (from 83.37% to 88.65%) under SFDA-Noise and by 1.67% (from 88.97% to 90.64%) under MT-Noise, compared to the baseline.

Furthermore, as illustrated in Fig. 3, qualitative results from the top four methods ranked by Dice under MT-Noise confirm the effectiveness of our approach in producing accurate and robust segmentation outputs.

##### 4.5.2 Results on the Pancreas-CT dataset

Table 2 present the quantitative comparison results on the Pancreas-CT[36] with two different noise types: SFDA noise (denoted as SFDA-Noise) and morphologically transformed noise (denoted as MT-Noise).

Our proposed SVL-DRL achieving state-of-the-art results across both noise settings. Specifically, our method improves the Dice score by 4.33% (from 74.31% to 78.64%) under SFDA-Noise and by 3.11% (from 78.41% to 81.52%) under MT-Noise, compared to the baseline. Notably, under MT-Noise, our method even surpasses the baseline model trained on clean labels (79.19% vs. 81.52% in Dice), demonstrating strong denoising and generalization capabilities. In terms of model performance, 50% MT-noise training data did not cause significant changes in the performance of the baseline model.

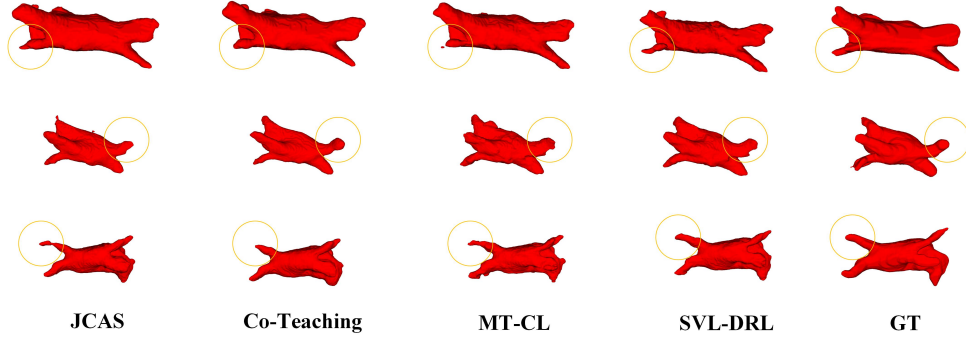


**Fig. 3** Visual comparison of segmentation results on the LA dataset under MT-noise label setting across different methods.

**Table 1** Segmentation performance comparison under different noise conditions on the LA dataset[35].

	Method	Dice[%] $\uparrow$	IoU[%] $\uparrow$	HD95[mm] $\downarrow$	ASD[mm] $\downarrow$
<b>clean</b>	Baseline	91.61( $\pm$ 0.10)	84.59( $\pm$ 0.13)	2.58( $\pm$ 0.74)	1.41( $\pm$ 0.08)
	Baseline	83.37( $\pm$ 0.18)	71.49( $\pm$ 0.23)	13.68( $\pm$ 1.90)	6.78( $\pm$ 0.28)
<b>SFDA-Noise</b>	Loss Correction[12]	84.06( $\pm$ 0.19)	72.50( $\pm$ 0.26)	12.26( $\pm$ 1.83)	6.71( $\pm$ 0.18)
	Co-Teaching[14]	85.69( $\pm$ 0.16)	74.95( $\pm$ 0.18)	10.49( $\pm$ 1.88)	5.12( $\pm$ 0.17)
	MTCL[23]	86.47( $\pm$ 0.18)	76.17( $\pm$ 0.18)	9.48( $\pm$ 1.78)	5.72( $\pm$ 0.17)
	ADELE[24]	85.28( $\pm$ 0.23)	74.33( $\pm$ 0.25)	10.05( $\pm$ 1.09)	5.18( $\pm$ 0.21)
	JCAS[16]	86.39( $\pm$ 0.15)	76.03( $\pm$ 0.17)	9.93( $\pm$ 1.83)	5.51( $\pm$ 0.50)
	RSF-Assisted[25]	85.92( $\pm$ 0.16)	75.32( $\pm$ 0.18)	11.92( $\pm$ 1.71)	6.46( $\pm$ 0.33)
	CLCS[18]	87.09( $\pm$ 0.15)	77.15( $\pm$ 0.17)	8.17( $\pm$ 1.86)	4.05( $\pm$ 0.48)
	<b>SVL-DRL(ours)</b>	<b>88.65(<math>\pm</math>0.14)</b>	<b>79.62(<math>\pm</math>0.16)</b>	<b>6.55(<math>\pm</math>1.83)</b>	<b>2.23(<math>\pm</math>0.18)</b>
<b>MT-Noise</b>	Baseline	88.97( $\pm$ 0.26)	80.43( $\pm$ 0.25)	6.24( $\pm$ 1.05)	1.80( $\pm$ 0.62)
	Loss Correction[12]	89.13( $\pm$ 0.22)	80.39( $\pm$ 0.26)	5.63( $\pm$ 0.83)	2.01( $\pm$ 0.47)
	Co-Teaching[14]	90.39( $\pm$ 0.25)	82.60( $\pm$ 0.31)	4.40( $\pm$ 0.84)	1.53( $\pm$ 0.19)
	MTCL[23]	90.47( $\pm$ 0.19)	82.60( $\pm$ 0.26)	4.57( $\pm$ 0.25)	1.55( $\pm$ 0.28)
	ADELE[24]	89.42( $\pm$ 0.23)	80.87( $\pm$ 0.26)	5.05( $\pm$ 1.64)	1.89( $\pm$ 0.72)
	JCAS[16]	90.28( $\pm$ 0.18)	82.28( $\pm$ 0.18)	4.12( $\pm$ 0.59)	1.64( $\pm$ 0.25)
	RSF-Assisted[25]	90.14( $\pm$ 0.20)	82.05( $\pm$ 0.23)	5.79( $\pm$ 0.65)	1.58( $\pm$ 0.11)
	CLCS[18]	89.84( $\pm$ 0.24)	81.57( $\pm$ 0.24)	5.54( $\pm$ 0.92)	1.83( $\pm$ 0.40)
<b>SVL-DRL(ours)</b>	<b>90.64(<math>\pm</math>0.13)</b>	<b>82.95(<math>\pm</math>0.11)</b>	<b>3.80(<math>\pm</math>0.36)</b>	<b>1.48(<math>\pm</math>0.38)</b>	

Furthermore, as illustrated in Fig. 4, qualitative results from the top four methods ranked by Dice under MT-Noise confirm the effectiveness of our approach in producing accurate and robust segmentation outputs.

### 4.5.3 Results on the BraTS 2021 dataset

Table 3 and Table 4 present the quantitative comparison results on the BraTS 2021 dataset[39] with two different noise types: SFDA noise (denoted as SFDA-Noise) and morphologically transformed noise (denoted as MT-Noise). Under the typical supervised baseline setting, the baseline network achieves poor performance on both Dice and IoU with different types of noisy labels used as ground truth labels. All label-noise robust learning methods outperform the baseline, with our proposed SVL-DRL achieving state-of-the-art results across both noise settings. Specifically, our method

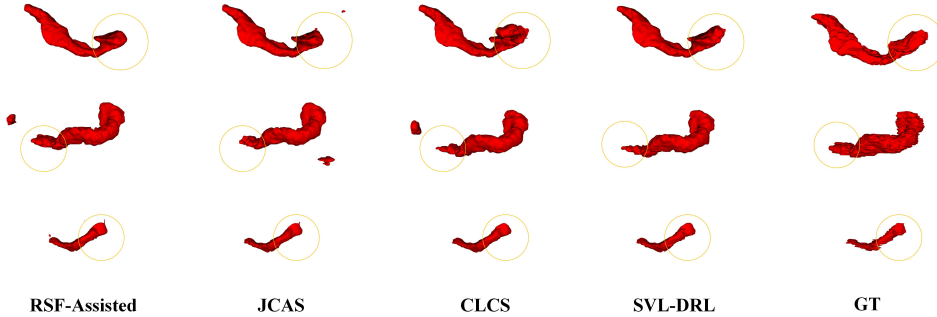


**Fig. 4** Visual comparison of segmentation results on the Pancreas dataset under MT-noise label setting across different methods.

**Table 2** Segmentation performance comparison under different noise conditions on the Pancreas-CT[36].

	Method	Dice[%] $\uparrow$	IoU[%] $\uparrow$	HD95[mm] $\downarrow$	ASD[mm] $\downarrow$
<b>clean</b>	Baseline	79.19( $\pm 0.15$ )	66.43( $\pm 0.13$ )	17.69( $\pm 1.06$ )	2.80( $\pm 0.15$ )
	Baseline	74.31( $\pm 0.29$ )	59.12( $\pm 0.30$ )	27.92( $\pm 1.21$ )	5.07( $\pm 0.38$ )
<b>SFDA-Noise</b>	Loss Correction[12]	75.12( $\pm 0.24$ )	60.15( $\pm 0.24$ )	26.73( $\pm 2.13$ )	4.83( $\pm 0.60$ )
	Co-Teaching[14]	77.35( $\pm 0.27$ )	63.07( $\pm 0.24$ )	20.08( $\pm 2.64$ )	3.69( $\pm 0.81$ )
	MTCL[23]	76.93( $\pm 0.23$ )	62.51( $\pm 0.25$ )	24.37( $\pm 2.22$ )	3.87( $\pm 0.64$ )
	ADELE[24]	77.17( $\pm 0.31$ )	62.83( $\pm 0.35$ )	21.41( $\pm 1.83$ )	4.16( $\pm 0.50$ )
	JCAS[16]	77.59( $\pm 0.29$ )	63.38( $\pm 0.32$ )	19.64( $\pm 2.14$ )	3.41( $\pm 0.60$ )
	RSF-Assisted[25]	76.21( $\pm 0.28$ )	61.56( $\pm 0.21$ )	23.17( $\pm 1.62$ )	4.04( $\pm 0.42$ )
	CLCS[18]	77.89( $\pm 0.26$ )	63.78( $\pm 0.28$ )	19.83( $\pm 1.45$ )	3.26( $\pm 0.31$ )
	<b>SVL-DRL(ours)</b>	<b>78.64(<math>\pm 0.20</math>)</b>	<b>64.81(<math>\pm 0.22</math>)</b>	<b>17.32(<math>\pm 1.46</math>)</b>	<b>2.86(<math>\pm 0.41</math>)</b>
<b>MT-Noise</b>	Baseline	78.41( $\pm 0.18$ )	65.23( $\pm 0.23$ )	18.53( $\pm 1.32$ )	2.98( $\pm 0.27$ )
	Loss Correction[12]	78.63( $\pm 0.17$ )	64.79( $\pm 0.21$ )	19.48( $\pm 1.42$ )	3.07( $\pm 0.29$ )
	Co-Teaching[14]	79.10( $\pm 0.20$ )	66.21( $\pm 0.24$ )	21.41( $\pm 1.37$ )	3.20( $\pm 0.18$ )
	MTCL[23]	79.21( $\pm 0.28$ )	65.58( $\pm 0.21$ )	13.25( $\pm 1.79$ )	2.79( $\pm 0.33$ )
	ADELE[24]	78.89( $\pm 0.16$ )	65.13( $\pm 0.19$ )	17.92( $\pm 1.56$ )	2.98( $\pm 0.27$ )
	JCAS[16]	80.12( $\pm 0.22$ )	66.83( $\pm 0.24$ )	8.69( $\pm 1.25$ )	2.73( $\pm 0.16$ )
	RSF-Assisted[25]	79.69( $\pm 0.23$ )	66.23( $\pm 0.24$ )	13.57( $\pm 1.91$ )	3.12( $\pm 0.36$ )
	CLCS[18]	80.47( $\pm 0.24$ )	67.32( $\pm 0.29$ )	8.05( $\pm 1.44$ )	2.81( $\pm 0.21$ )
<b>SVL-DRL(ours)</b>	<b>81.52(<math>\pm 0.16</math>)</b>	<b>69.22(<math>\pm 0.18</math>)</b>	<b>5.91(<math>\pm 1.28</math>)</b>	<b>2.04(<math>\pm 0.20</math>)</b>	

improves the Average Dice score by 3.95% (from 86.17% to 90.12%) under SFDA-Noise and by 3.14% (from 87.89% to 91.03%) under MT-Noise, compared to the baseline.

As illustrated in Fig. 5, qualitative results from the top four methods ranked by Dice under MT-Noise confirm the effectiveness of our approach in producing accurate and robust segmentation outputs.

#### 4.6 Impact of Noise Ratio

To investigate the influence of the noise ratio in the training set on model performance, we conducted training experiments on the LA dataset[35] with different ratios of noise. The performance of the baseline model under different noise data ratios is shown in Fig. 6. The line graph demonstrates a strong negative correlation between

**Table 3** Segmentation performance comparison under different noise conditions on the BraTS 2021 dataset[39].

	Method	ET		WT		TC		Average	
		Dice $\uparrow$	IoU $\uparrow$						
clean	Baseline	89.33( $\pm 0.12$ )	82.13( $\pm 0.15$ )	93.75( $\pm 0.08$ )	88.62( $\pm 0.10$ )	92.67( $\pm 0.09$ )	87.60( $\pm 0.11$ )	91.92( $\pm 0.10$ )	86.12( $\pm 0.12$ )
	Baseline	82.19( $\pm 0.18$ )	72.04( $\pm 0.22$ )	91.31( $\pm 0.15$ )	84.58( $\pm 0.18$ )	85.01( $\pm 0.20$ )	76.07( $\pm 0.25$ )	86.17( $\pm 0.18$ )	77.56( $\pm 0.22$ )
	Loss Correction[12]	84.87( $\pm 0.16$ )	75.81( $\pm 0.19$ )	91.41( $\pm 0.14$ )	84.79( $\pm 0.16$ )	87.48( $\pm 0.17$ )	79.77( $\pm 0.20$ )	87.92( $\pm 0.16$ )	80.12( $\pm 0.18$ )
	Co-Teaching[14]	84.34( $\pm 0.15$ )	74.82( $\pm 0.18$ )	91.43( $\pm 0.13$ )	84.85( $\pm 0.15$ )	88.71( $\pm 0.16$ )	81.60( $\pm 0.19$ )	88.16( $\pm 0.15$ )	80.42( $\pm 0.17$ )
	MTCL[23]	84.76( $\pm 0.14$ )	75.43( $\pm 0.17$ )	91.49( $\pm 0.12$ )	84.85( $\pm 0.14$ )	88.70( $\pm 0.15$ )	81.51( $\pm 0.18$ )	88.32( $\pm 0.14$ )	80.60( $\pm 0.16$ )
	ADELE[24]	84.66( $\pm 0.17$ )	75.45( $\pm 0.20$ )	87.52( $\pm 0.19$ )	78.54( $\pm 0.22$ )	88.00( $\pm 0.18$ )	80.55( $\pm 0.21$ )	86.72( $\pm 0.18$ )	78.18( $\pm 0.21$ )
	JCAS[16]	85.36( $\pm 0.13$ )	76.15( $\pm 0.16$ )	92.01( $\pm 0.11$ )	85.75( $\pm 0.13$ )	88.37( $\pm 0.14$ )	80.93( $\pm 0.17$ )	88.58( $\pm 0.13$ )	80.94( $\pm 0.15$ )
	RSF-Assisted[25]	86.20( $\pm 0.12$ )	77.44( $\pm 0.15$ )	91.62( $\pm 0.10$ )	85.10( $\pm 0.12$ )	88.86( $\pm 0.13$ )	81.69( $\pm 0.16$ )	88.89( $\pm 0.12$ )	81.41( $\pm 0.14$ )
	CLCS[18]	85.52( $\pm 0.14$ )	76.49( $\pm 0.17$ )	91.59( $\pm 0.11$ )	85.02( $\pm 0.13$ )	89.37( $\pm 0.12$ )	82.39( $\pm 0.15$ )	88.83( $\pm 0.13$ )	81.30( $\pm 0.15$ )
SVL-DRL(ours)	<b>87.43(<math>\pm 0.10</math>)</b>	<b>79.42(<math>\pm 0.12</math>)</b>	<b>92.52(<math>\pm 0.08</math>)</b>	<b>86.59(<math>\pm 0.10</math>)</b>	<b>90.42(<math>\pm 0.09</math>)</b>	<b>84.20(<math>\pm 0.11</math>)</b>	<b>90.12(<math>\pm 0.09</math>)</b>	<b>83.40(<math>\pm 0.11</math>)</b>	
SFDA-Noise	Baseline	85.56( $\pm 0.20$ )	76.91( $\pm 0.24$ )	91.50( $\pm 0.17$ )	84.82( $\pm 0.20$ )	86.60( $\pm 0.22$ )	78.77( $\pm 0.26$ )	87.89( $\pm 0.20$ )	80.17( $\pm 0.23$ )
	Loss Correction[12]	85.90( $\pm 0.18$ )	77.24( $\pm 0.21$ )	92.00( $\pm 0.15$ )	85.64( $\pm 0.18$ )	89.44( $\pm 0.19$ )	82.80( $\pm 0.22$ )	89.11( $\pm 0.18$ )	81.90( $\pm 0.20$ )
	Co-Teaching[14]	85.59( $\pm 0.19$ )	76.83( $\pm 0.23$ )	91.78( $\pm 0.16$ )	85.42( $\pm 0.19$ )	88.96( $\pm 0.20$ )	82.22( $\pm 0.24$ )	88.78( $\pm 0.19$ )	81.49( $\pm 0.22$ )
	MTCL[23]	87.52( $\pm 0.15$ )	79.34( $\pm 0.18$ )	92.87( $\pm 0.12$ )	87.16( $\pm 0.14$ )	90.88( $\pm 0.16$ )	84.74( $\pm 0.19$ )	90.42( $\pm 0.15$ )	83.75( $\pm 0.17$ )
	ADELE[24]	87.94( $\pm 0.16$ )	80.00( $\pm 0.19$ )	90.09( $\pm 0.18$ )	82.91( $\pm 0.21$ )	91.15( $\pm 0.17$ )	85.11( $\pm 0.20$ )	89.73( $\pm 0.17$ )	82.67( $\pm 0.20$ )
	JCAS[16]	87.00( $\pm 0.17$ )	78.76( $\pm 0.20$ )	91.64( $\pm 0.16$ )	85.12( $\pm 0.19$ )	89.86( $\pm 0.18$ )	83.42( $\pm 0.21$ )	89.50( $\pm 0.17$ )	82.44( $\pm 0.20$ )
	RSF-Assisted[25]	87.41( $\pm 0.14$ )	79.44( $\pm 0.17$ )	92.70( $\pm 0.13$ )	86.90( $\pm 0.15$ )	89.99( $\pm 0.15$ )	83.79( $\pm 0.18$ )	90.04( $\pm 0.14$ )	83.38( $\pm 0.16$ )
	CLCS[18]	87.99( $\pm 0.13$ )	80.07( $\pm 0.15$ )	92.78( $\pm 0.11$ )	86.98( $\pm 0.13$ )	<b>91.92(<math>\pm 0.10</math>)</b>	<b>86.27(<math>\pm 0.12</math>)</b>	90.89( $\pm 0.11$ )	84.44( $\pm 0.13$ )
	SVL-DRL(ours)	<b>88.32(<math>\pm 0.11</math>)</b>	<b>80.80(<math>\pm 0.13</math>)</b>	<b>93.10(<math>\pm 0.09</math>)</b>	<b>87.58(<math>\pm 0.11</math>)</b>	91.67( $\pm 0.10$ )	86.20( $\pm 0.12$ )	<b>91.03(<math>\pm 0.10</math>)</b>	<b>84.86(<math>\pm 0.12</math>)</b>
MT-Noise	Baseline	85.56( $\pm 0.20$ )	76.91( $\pm 0.24$ )	91.50( $\pm 0.17$ )	84.82( $\pm 0.20$ )	86.60( $\pm 0.22$ )	78.77( $\pm 0.26$ )	87.89( $\pm 0.20$ )	80.17( $\pm 0.23$ )
	Loss Correction[12]	85.90( $\pm 0.18$ )	77.24( $\pm 0.21$ )	92.00( $\pm 0.15$ )	85.64( $\pm 0.18$ )	89.44( $\pm 0.19$ )	82.80( $\pm 0.22$ )	89.11( $\pm 0.18$ )	81.90( $\pm 0.20$ )
	Co-Teaching[14]	85.59( $\pm 0.19$ )	76.83( $\pm 0.23$ )	91.78( $\pm 0.16$ )	85.42( $\pm 0.19$ )	88.96( $\pm 0.20$ )	82.22( $\pm 0.24$ )	88.78( $\pm 0.19$ )	81.49( $\pm 0.22$ )
	MTCL[23]	87.52( $\pm 0.15$ )	79.34( $\pm 0.18$ )	92.87( $\pm 0.12$ )	87.16( $\pm 0.14$ )	90.88( $\pm 0.16$ )	84.74( $\pm 0.19$ )	90.42( $\pm 0.15$ )	83.75( $\pm 0.17$ )
	ADELE[24]	87.94( $\pm 0.16$ )	80.00( $\pm 0.19$ )	90.09( $\pm 0.18$ )	82.91( $\pm 0.21$ )	91.15( $\pm 0.17$ )	85.11( $\pm 0.20$ )	89.73( $\pm 0.17$ )	82.67( $\pm 0.20$ )
	JCAS[16]	87.00( $\pm 0.17$ )	78.76( $\pm 0.20$ )	91.64( $\pm 0.16$ )	85.12( $\pm 0.19$ )	89.86( $\pm 0.18$ )	83.42( $\pm 0.21$ )	89.50( $\pm 0.17$ )	82.44( $\pm 0.20$ )
	RSF-Assisted[25]	87.41( $\pm 0.14$ )	79.44( $\pm 0.17$ )	92.70( $\pm 0.13$ )	86.90( $\pm 0.15$ )	89.99( $\pm 0.15$ )	83.79( $\pm 0.18$ )	90.04( $\pm 0.14$ )	83.38( $\pm 0.16$ )
	CLCS[18]	87.99( $\pm 0.13$ )	80.07( $\pm 0.15$ )	92.78( $\pm 0.11$ )	86.98( $\pm 0.13$ )	<b>91.92(<math>\pm 0.10</math>)</b>	<b>86.27(<math>\pm 0.12</math>)</b>	90.89( $\pm 0.11$ )	84.44( $\pm 0.13$ )
	SVL-DRL(ours)	<b>88.32(<math>\pm 0.11</math>)</b>	<b>80.80(<math>\pm 0.13</math>)</b>	<b>93.10(<math>\pm 0.09</math>)</b>	<b>87.58(<math>\pm 0.11</math>)</b>	91.67( $\pm 0.10$ )	86.20( $\pm 0.12$ )	<b>91.03(<math>\pm 0.10</math>)</b>	<b>84.86(<math>\pm 0.12</math>)</b>

**Table 4** Segmentation performance comparison under different noise conditions on the BraTS 2021 dataset[39].

	Method	ET		WT		TC		Average	
		HD95 $\downarrow$	ASD $\downarrow$						
clean	Baseline	3.84( $\pm 0.28$ )	1.45( $\pm 0.12$ )	6.93( $\pm 0.35$ )	2.09( $\pm 0.18$ )	4.44( $\pm 0.31$ )	1.37( $\pm 0.11$ )	5.07( $\pm 0.32$ )	1.64( $\pm 0.14$ )
	Baseline	6.48( $\pm 0.52$ )	2.01( $\pm 0.16$ )	8.37( $\pm 0.41$ )	2.36( $\pm 0.19$ )	7.96( $\pm 0.48$ )	2.18( $\pm 0.17$ )	7.60( $\pm 0.47$ )	2.18( $\pm 0.18$ )
	Loss Correction[12]	6.47( $\pm 0.49$ )	1.85( $\pm 0.15$ )	9.49( $\pm 0.45$ )	2.50( $\pm 0.20$ )	7.60( $\pm 0.46$ )	1.94( $\pm 0.16$ )	7.86( $\pm 0.44$ )	2.10( $\pm 0.17$ )
	Co-Teaching[14]	5.61( $\pm 0.43$ )	1.74( $\pm 0.14$ )	8.35( $\pm 0.39$ )	2.39( $\pm 0.18$ )	6.14( $\pm 0.38$ )	1.72( $\pm 0.13$ )	6.70( $\pm 0.40$ )	1.95( $\pm 0.15$ )
	MTCL[23]	5.73( $\pm 0.44$ )	1.79( $\pm 0.14$ )	9.13( $\pm 0.42$ )	2.41( $\pm 0.19$ )	6.71( $\pm 0.41$ )	1.78( $\pm 0.14$ )	7.19( $\pm 0.42$ )	1.99( $\pm 0.16$ )
	ADELE[24]	6.77( $\pm 0.51$ )	1.96( $\pm 0.16$ )	16.91( $\pm 0.68$ )	3.42( $\pm 0.27$ )	9.59( $\pm 0.53$ )	2.18( $\pm 0.18$ )	11.09( $\pm 0.57$ )	2.52( $\pm 0.21$ )
	JCAS[16]	5.83( $\pm 0.45$ )	1.69( $\pm 0.13$ )	8.89( $\pm 0.41$ )	2.41( $\pm 0.19$ )	7.34( $\pm 0.43$ )	1.86( $\pm 0.15$ )	7.35( $\pm 0.43$ )	1.99( $\pm 0.16$ )
	RSF-Assisted[25]	5.32( $\pm 0.41$ )	1.67( $\pm 0.13$ )	7.98( $\pm 0.38$ )	2.34( $\pm 0.18$ )	6.67( $\pm 0.40$ )	1.75( $\pm 0.14$ )	6.66( $\pm 0.40$ )	1.92( $\pm 0.15$ )
	CLCS[18]	5.25( $\pm 0.40$ )	1.68( $\pm 0.13$ )	7.77( $\pm 0.37$ )	2.26( $\pm 0.17$ )	6.21( $\pm 0.38$ )	1.69( $\pm 0.13$ )	6.41( $\pm 0.38$ )	1.88( $\pm 0.15$ )
SVL-DRL(ours)	<b>4.81(<math>\pm 0.36</math>)</b>	<b>1.58(<math>\pm 0.12</math>)</b>	<b>8.36(<math>\pm 0.35</math>)</b>	<b>2.32(<math>\pm 0.16</math>)</b>	<b>5.71(<math>\pm 0.34</math>)</b>	<b>1.58(<math>\pm 0.11</math>)</b>	<b>6.29(<math>\pm 0.35</math>)</b>	<b>1.82(<math>\pm 0.13</math>)</b>	
SFDA-Noise	Baseline	7.82( $\pm 0.58$ )	1.97( $\pm 0.17$ )	10.63( $\pm 0.49$ )	2.53( $\pm 0.21$ )	10.40( $\pm 0.52$ )	2.31( $\pm 0.19$ )	9.61( $\pm 0.53$ )	2.27( $\pm 0.20$ )
	Loss Correction[12]	8.00( $\pm 0.56$ )	2.03( $\pm 0.17$ )	9.28( $\pm 0.46$ )	2.40( $\pm 0.20$ )	9.29( $\pm 0.50$ )	2.01( $\pm 0.18$ )	8.86( $\pm 0.51$ )	2.15( $\pm 0.19$ )
	Co-Teaching[14]	7.23( $\pm 0.53$ )	1.97( $\pm 0.16$ )	8.70( $\pm 0.44$ )	2.44( $\pm 0.19$ )	8.86( $\pm 0.48$ )	2.03( $\pm 0.17$ )	8.27( $\pm 0.48$ )	2.15( $\pm 0.18$ )
	MTCL[23]	4.44( $\pm 0.35$ )	1.55( $\pm 0.11$ )	7.51( $\pm 0.38$ )	2.20( $\pm 0.16$ )	5.87( $\pm 0.36$ )	1.53( $\pm 0.10$ )	5.94( $\pm 0.36$ )	1.76( $\pm 0.13$ )
	ADELE[24]	<b>4.40(<math>\pm 0.34</math>)</b>	<b>1.56(<math>\pm 0.11</math>)</b>	18.88( $\pm 0.72$ )	3.67( $\pm 0.29$ )	5.14( $\pm 0.33$ )	1.51( $\pm 0.10$ )	9.48( $\pm 0.46$ )	2.25( $\pm 0.18$ )
	JCAS[16]	4.99( $\pm 0.38$ )	1.64( $\pm 0.12$ )	8.79( $\pm 0.42$ )	2.44( $\pm 0.18$ )	5.97( $\pm 0.37$ )	1.63( $\pm 0.11$ )	6.58( $\pm 0.39$ )	1.90( $\pm 0.14$ )
	RSF-Assisted[25]	4.83( $\pm 0.37$ )	1.61( $\pm 0.12$ )	7.35( $\pm 0.36$ )	2.20( $\pm 0.15$ )	5.60( $\pm 0.35$ )	1.63( $\pm 0.11$ )	5.92( $\pm 0.36$ )	1.81( $\pm 0.13$ )
	CLCS[18]	4.58( $\pm 0.35$ )	1.56( $\pm 0.11$ )	8.51( $\pm 0.40$ )	2.30( $\pm 0.17$ )	5.16( $\pm 0.32$ )	1.50( $\pm 0.10$ )	6.08( $\pm 0.36$ )	1.79( $\pm 0.13$ )
	SVL-DRL(ours)	4.56( $\pm 0.33$ )	<b>1.53(<math>\pm 0.10</math>)</b>	<b>7.30(<math>\pm 0.34</math>)</b>	<b>2.18(<math>\pm 0.14</math>)</b>	<b>5.13(<math>\pm 0.31</math>)</b>	<b>1.48(<math>\pm 0.09</math>)</b>	<b>5.66(<math>\pm 0.33</math>)</b>	<b>1.74(<math>\pm 0.12</math>)</b>
MT-Noise	Baseline	7.82( $\pm 0.58$ )	1.97( $\pm 0.17$ )	10.63( $\pm 0.49$ )	2.53( $\pm 0.21$ )	10.40( $\pm 0.52$ )	2.31( $\pm 0.19$ )	9.61( $\pm 0.53$ )	2.27( $\pm 0.20$ )
	Loss Correction[12]	8.00( $\pm 0.56$ )	2.03( $\pm 0.17$ )	9.28( $\pm 0.46$ )	2.40( $\pm 0.20$ )	9.29( $\pm 0.50$ )	2.01( $\pm 0.18$ )	8.86( $\pm 0.51$ )	2.15( $\pm 0.19$ )
	Co-Teaching[14]	7.23( $\pm 0.53$ )	1.97( $\pm 0.16$ )	8.70( $\pm 0.44$ )	2.44( $\pm 0.19$ )	8.86( $\pm 0.48$ )	2.03( $\pm 0.17$ )	8.27( $\pm 0.48$ )	2.15( $\pm 0.18$ )
	MTCL[23]	4.44( $\pm 0.35$ )	1.55( $\pm 0.11$ )	7.51( $\pm 0.38$ )	2.20( $\pm 0.16$ )	5.87( $\pm 0.36$ )	1.53( $\pm 0.10$ )	5.94( $\pm 0.36$ )	1.76( $\pm 0.13$ )
	ADELE[24]	<b>4.40(<math>\pm 0.34</math>)</b>	<b>1.56(<math>\pm 0.11</math>)</b>	18.88( $\pm 0.72$ )	3.67( $\pm 0.29$ )	5.14( $\pm 0.33$ )	1.51( $\pm 0.10$ )	9.48( $\pm 0.46$ )	2.25( $\pm 0.18$ )
	JCAS[16]	4.99( $\pm 0.38$ )	1.64( $\pm 0.12$ )	8.79( $\pm 0.42$ )	2.44( $\pm 0.18$ )	5.97( $\pm 0.37$ )	1.63( $\pm 0.11$ )	6.58( $\pm 0.39$ )	1.90( $\pm 0.14$ )
	RSF-Assisted[25]	4.83( $\pm 0.37$ )	1.61( $\pm 0.12$ )	7.35( $\pm 0.36$ )	2.20( $\pm 0.15$ )	5.60( $\pm 0.35$ )	1.63( $\pm 0.11$ )	5.92( $\pm 0.36$ )	1.81( $\pm 0.13$ )
	CLCS[18]	4.58( $\pm 0.35$ )	1.56( $\pm 0.11$ )	8.51( $\pm 0.40$ )	2.30( $\pm 0.17$ )	5.16( $\pm 0.32$ )	1.50( $\pm 0.10$ )	6.08( $\pm 0.36$ )	1.79( $\pm 0.13$ )
	SVL-DRL(ours)	4.56( $\pm 0.33$ )	<b>1.53(<math>\pm 0.10</math>)</b>	<b>7.30(<math>\pm 0.34</math>)</b>	<b>2.18(<math>\pm 0.14</math>)</b>	<b>5.13(<math>\pm 0.31</math>)</b>	<b>1.48(<math>\pm 0.09</math>)</b>	<b>5.66(<math>\pm 0.33</math>)</b>	<b>1.74(<math>\pm 0.12</math>)</b>

the noise ratio in the training set and the model’s Dice coefficient. As evident from the results, our model demonstrates a slower decay in Dice values with increasing noise levels, indicating superior robustness against noise corruption.

## 4.7 Ablation Studies

To evaluate the effectiveness of each component of the proposed method, we conducted extensive experiments on LA dataset[35] and Pancreas dataset[36] with two different noise types. As shown in Table5 and Table6. Swin Unetr[19] was used as the baseline for ablation studies. The experiments included: 1) SVL-DRL w/o WS: the framework without Warmup Stage(WS); 2) SVL-DRL w/o TS: the framework without Transition Stage(TS); 3) SVL-DRL w/o WAT: the framework without Warmup Stage and Transition Stage(WAT); 4) SVL-DRL w/o FRL: the framework without Full RL Stage(FRL).

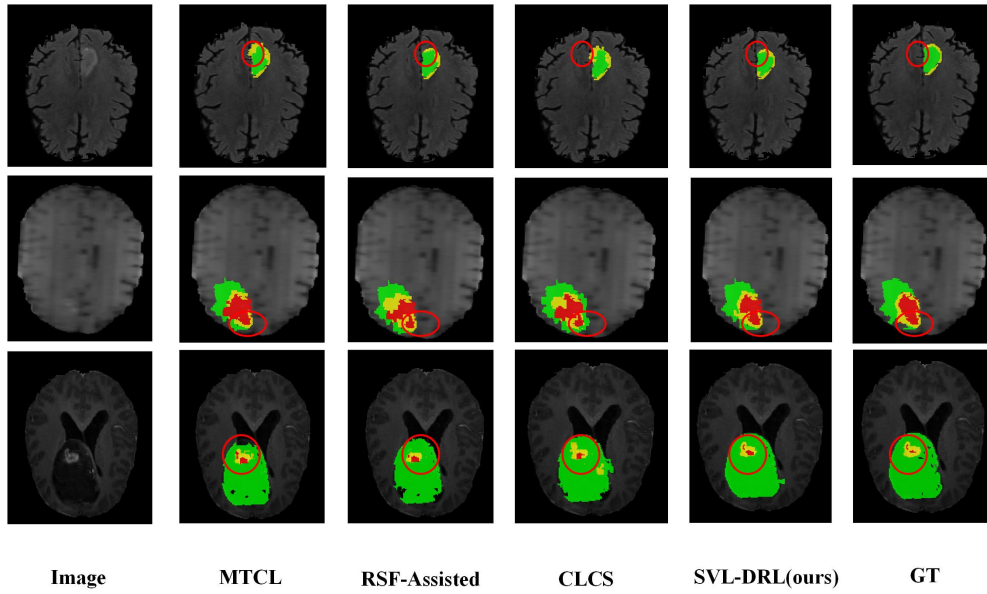


**Fig. 5** Visual comparison of segmentation results on the BraTS 2021 dataset under MT-noise label setting across different methods.

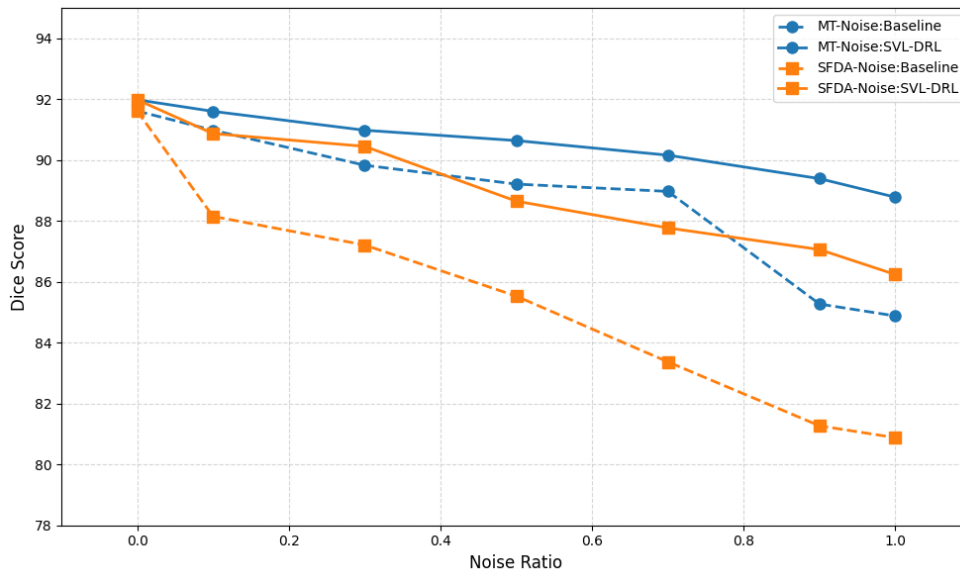


**Fig. 6** The performance of SVL-DRL and baseline model under different noise data ratios in the LA dataset[35].

**Table 5** Ablation Study on LA Dataset

	Method	Dice	IoU	HD95	ASD
<b>SFDA-Noise</b>	Baseline	83.37	71.49	13.68	6.78
	SVL-DRL w/o WS	80.34	67.14	9.07	4.89
	SVL-DRL w/o TS	86.19	75.69	7.92	3.67
	SVL-DRL w/o WAT	76.21	61.54	23.52	11.06
	SVL-DRL w/o FRL	84.93	73.68	8.63	3.91
	<b>SVL-DRL(ours)</b>	<b>88.65</b>	<b>79.62</b>	<b>6.55</b>	<b>2.23</b>
<b>MT-Noise</b>	Baseline	88.97	80.43	6.24	1.80
	SVL-DRL w/o WS	82.13	69.66	13.58	8.63
	SVL-DRL w/o TS	89.14	80.43	5.84	1.69
	SVL-DRL w/o WAT	80.47	67.31	13.37	4.81
	SVL-DRL w/o FRL	89.28	80.62	5.42	1.73
	<b>SVL-DRL(ours)</b>	<b>90.64</b>	<b>82.95</b>	<b>3.80</b>	<b>1.48</b>

**Table 6** Ablation Study on Pancreas Dataset

	Method	Dice	IoU	HD95	ASD
<b>SFDA-Noise</b>	Baseline	74.31	59.12	27.92	5.07
	SVL-DRL w/o WS	71.76	55.96	31.28	7.92
	SVL-DRL w/o TS	74.33	59.14	28.06	4.97
	SVL-DRL w/o WAT	69.14	52.84	35.49	8.41
	SVL-DRL w/o FRL	76.58	62.03	21.83	3.24
	<b>SVL-DRL(ours)</b>	<b>78.64</b>	<b>64.81</b>	<b>17.32</b>	<b>2.86</b>
<b>MT-Noise</b>	Baseline	78.41	65.23	18.53	2.98
	SVL-DRL w/o WS	76.12	61.45	22.48	3.59
	SVL-DRL w/o TS	78.95	65.22	21.65	3.24
	SVL-DRL w/o WAT	75.49	60.63	29.04	3.97
	SVL-DRL w/o FRL	80.26	67.01	18.02	2.56
	<b>SVL-DRL(ours)</b>	<b>81.52</b>	<b>69.22</b>	<b>5.91</b>	<b>2.04</b>

As shown in Table 5 and Table 6, the performance of the framework without Warmup Stage is even lower than the baseline, and our analysis is that reinforcement learning requires correct semantic information guidance. Warm Stage is an important stage for the entire segmentation task, both Warm Stage and two other stages of training can achieve significant results.

## 5 Discussion

This study presents a novel deep reinforcement learning framework designed to mitigate the impact of noisy labels in 3D medical image segmentation. Experimental evaluations confirm that the proposed method yields substantial improvements over existing baseline models. A key aspect of our framework is the incorporation of voxel-level action spaces and reward functions specifically adapted to the characteristics of medical imaging data.

Unlike existing strategies such as MS-TAAL [26] and CLCL [18], which attempt to alleviate label noise by filtering out unreliable annotations, our approach seeks to directly correct noisy labels through a reward-based learning mechanism. Methods that depend on clean-label selection may inadvertently discard useful semantic information contained in imperfect annotations, thereby limiting their learning potential. In contrast, our framework retains and refines noisy labels by leveraging an

action-reward mechanism, enabling the model to learn from all available data while dynamically adjusting label quality. This capacity to progressively correct label inaccuracies—rather than excluding them—likely accounts for the notable performance advantage observed in our comparative experiments.

## 6 Conclusion

This paper introduces an end-to-end staged voxel-level deep reinforcement learning framework (SVL-DRL), which is designed for 3D noise-robust medical image segmentation. The framework autonomously mitigates the adverse effects of noisy labels on segmentation performance without requiring prior filtering or manual intervention. Additionally, we introduce a voxel-level asynchronous advantage actor-critic (vA3C) module, which enables dynamic refinement of input states without discarding any training samples. Comprehensive experiments on three public datasets demonstrate the effectiveness of each component in our proposed approach. Compared to the state-of-the-art methods, our framework demonstrates superior performance and robust competitiveness in managing noisy label data.

## References

- [1] Alotaibi, A.: Ensemble deep learning approaches in health care: A review. *Computers, Materials & Continua* **82**(3) (2025)
- [2] Obuchowicz, R., Strzelecki, M., Piórkowski, A.: Clinical applications of artificial intelligence in medical imaging and image processing—A review. *MDPI* (2024)
- [3] Kalita, A.J., Boruah, A., Das, T., Mazumder, N., Jaiswal, S.K., Zhuo, G.-Y., Gogoi, A., Kakoty, N.M., Kao, F.-J.: Artificial intelligence in diagnostic medical image processing for advanced healthcare applications. In: *Biomedical Imaging: Advances in Artificial Intelligence and Machine Learning*, pp. 1–61. Springer, ??? (2024)
- [4] Ashraf, M., Zaman, M.: Revealing historical insights: A comprehensive exploration of traditional approaches in medical image segmentation. *Deep Learning Applications in Medical Image Segmentation: Overview, Approaches, and Challenges*, 65–84 (2025)
- [5] Panayides, A.S., Amini, A., Filipovic, N.D., Sharma, A., Tsaftaris, S.A., Young, A., Foran, D., Do, N., Golemati, S., Kurc, T., *et al.*: Ai in medical imaging informatics: current challenges and future directions. *IEEE journal of biomedical and health informatics* **24**(7), 1837–1857 (2020)
- [6] Liu, X., Song, L., Liu, S., Zhang, Y.: A review of deep-learning-based medical image segmentation methods. *Sustainability* **13**(3), 1224 (2021)
- [7] Shobayo, O., Saatchi, R.: Developments in deep learning artificial neural network techniques for medical image analysis and interpretation. *Diagnostics* **15**(9), 1072

(2025)

- [8] Bach, J., Grohsjean, A., Schwanenberger, C., Stelldinger, P.: Unlearning with partial label learning. In: Proceedings of the 18th ACM International Conference on Pervasive Technologies Related to Assistive Environments, pp. 175–181 (2025)
- [9] Suyal, H., Singh, A.: A systematic literature survey of crowdsourcing: Current status and future perspectives. *Wiley Interdisciplinary Reviews: Data Mining and Knowledge Discovery* **15**(3), 70037 (2025)
- [10] Birjais, R.: Challenges and future directions for segmentation of medical images using deep learning models. *Deep Learning Applications in Medical Image Segmentation: Overview, Approaches, and Challenges*, 243–264 (2025)
- [11] Song, B., Zhao, S., Dang, L., Wang, H., Xu, L.: A survey on learning from data with label noise via deep neural networks. *Systems Science & Control Engineering* **13**(1), 2488120 (2025)
- [12] Patrini, G., Rozza, A., Krishna Menon, A., Nock, R., Qu, L.: Making deep neural networks robust to label noise: A loss correction approach. In: Proceedings of the IEEE Conference on Computer Vision and Pattern Recognition, pp. 1944–1952 (2017)
- [13] Li, X., Liu, T., Han, B., Niu, G., Sugiyama, M.: Provably end-to-end label-noise learning without anchor points. In: International Conference on Machine Learning, pp. 6403–6413 (2021). PMLR
- [14] Han, B., Yao, Q., Yu, X., Niu, G., Xu, M., Hu, W., Tsang, I., Sugiyama, M.: Co-teaching: Robust training of deep neural networks with extremely noisy labels. *Advances in neural information processing systems* **31** (2018)
- [15] Northcutt, C., Jiang, L., Chuang, I.: Confident learning: Estimating uncertainty in dataset labels. *Journal of Artificial Intelligence Research* **70**, 1373–1411 (2021)
- [16] Guo, X., Yuan, Y.: Joint class-affinity loss correction for robust medical image segmentation with noisy labels. In: International Conference on Medical Image Computing and Computer-assisted Intervention, pp. 588–598 (2022). Springer
- [17] Fang, C., Wang, Q., Cheng, L., Gao, Z., Pan, C., Cao, Z., Zheng, Z., Zhang, D.: Reliable mutual distillation for medical image segmentation under imperfect annotations. *IEEE Transactions on Medical Imaging* **42**(6), 1720–1734 (2023)
- [18] Guo, E., Wang, Z., Zhao, Z., Zhou, L.: Imbalanced medical image segmentation with pixel-dependent noisy labels. *IEEE Transactions on Medical Imaging* (2024)
- [19] Xiao, T., Xia, T., Yang, Y., Huang, C., Wang, X.: Learning from massive noisy labeled data for image classification. In: Proceedings of the IEEE Conference on

- Computer Vision and Pattern Recognition, pp. 2691–2699 (2015)
- [20] Huang, B., Xie, Y., Xu, C.: Learning with noisy labels via clean aware sharpness aware minimization. *Scientific Reports* **15**(1), 1350 (2025)
- [21] Nishi, K., Ding, Y., Rich, A., Hollerer, T.: Augmentation strategies for learning with noisy labels. In: *Proceedings of the IEEE/CVF Conference on Computer Vision and Pattern Recognition*, pp. 8022–8031 (2021)
- [22] Wang, Y., Liu, W., Ma, X., Bailey, J., Zha, H., Song, L., Xia, S.-T.: Iterative learning with open-set noisy labels. In: *Proceedings of the IEEE Conference on Computer Vision and Pattern Recognition*, pp. 8688–8696 (2018)
- [23] Xu, Z., Lu, D., Luo, J., Wang, Y., Yan, J., Ma, K., Zheng, Y., Tong, R.K.-Y.: Anti-interference from noisy labels: Mean-teacher-assisted confident learning for medical image segmentation. *IEEE Transactions on Medical Imaging* **41**(11), 3062–3073 (2022)
- [24] Liu, S., Liu, K., Zhu, W., Shen, Y., Fernandez-Granda, C.: Adaptive early-learning correction for segmentation from noisy annotations. In: *Proceedings of the IEEE/CVF Conference on Computer Vision and Pattern Recognition*, pp. 2606–2616 (2022)
- [25] Liu, S., Li, Y., Chai, Q.-w., Zheng, W.: Region-scalable fitting-assisted medical image segmentation with noisy labels. *Expert Systems with Applications* **238**, 121926 (2024)
- [26] Cui, B., Zhang, M., Xu, M., Wang, A., Yuan, W., Ren, H.: Rectifying noisy labels with sequential prior: Multi-scale temporal feature affinity learning for robust video segmentation. In: *International Conference on Medical Image Computing and Computer-Assisted Intervention*, pp. 90–100 (2023). Springer
- [27] Wang, L., Lekadir, K., Lee, S.-L., Merrifield, R., Yang, G.-Z.: A general framework for context-specific image segmentation using reinforcement learning. *IEEE transactions on medical imaging* **32**(5), 943–956 (2013)
- [28] Liao, X., Li, W., Xu, Q., Wang, X., Jin, B., Zhang, X., Wang, Y., Zhang, Y.: Iteratively-refined interactive 3d medical image segmentation with multi-agent reinforcement learning. In: *Proceedings of the IEEE/CVF Conference on Computer Vision and Pattern Recognition*, pp. 9394–9402 (2020)
- [29] Tian, Z., Si, X., Zheng, Y., Chen, Z., Li, X.: Multi-step medical image segmentation based on reinforcement learning. *Journal of Ambient Intelligence and Humanized Computing* **13**(11), 5011–5022 (2022)
- [30] Mnih, V., Badia, A.P., Mirza, M., Graves, A., Lillicrap, T., Harley, T., Silver, D., Kavukcuoglu, K.: Asynchronous methods for deep reinforcement learning. In:

International Conference on Machine Learning, pp. 1928–1937 (2016). PmLR

- [31] Frénay, B., Verleysen, M.: Classification in the presence of label noise: a survey. *IEEE transactions on neural networks and learning systems* **25**(5), 845–869 (2013)
- [32] Xiao, T., Xia, T., Yang, Y., Huang, C., Wang, X.: Learning from massive noisy labeled data for image classification. In: *Proceedings of the IEEE Conference on Computer Vision and Pattern Recognition*, pp. 2691–2699 (2015)
- [33] Yi, L., Xu, G., Xu, P., Li, J., Pu, R., Ling, C., McLeod, A.I., Wang, B.: When source-free domain adaptation meets learning with noisy labels. *arXiv preprint arXiv:2301.13381* (2023)
- [34] Li, S., Gao, Z., He, X.: Superpixel-guided iterative learning from noisy labels for medical image segmentation. In: *International Conference on Medical Image Computing and Computer-Assisted Intervention*, pp. 525–535 (2021). Springer
- [35] Xiong, Z., Xia, Q., Hu, Z., Huang, N., Bian, C., Zheng, Y., Vesal, S., Ravikumar, N., Maier, A., Yang, X., *et al.*: A global benchmark of algorithms for segmenting the left atrium from late gadolinium-enhanced cardiac magnetic resonance imaging. *Medical image analysis* **67**, 101832 (2021)
- [36] Clark, K., Vendt, B., Smith, K., Freymann, J., Kirby, J., Koppel, P., Moore, S., Phillips, S., Maffitt, D., Pringle, M., *et al.*: The cancer imaging archive (tcia): maintaining and operating a public information repository. *Journal of digital imaging* **26**(6), 1045–1057 (2013)
- [37] Luo, X., Chen, J., Song, T., Wang, G.: Semi-supervised medical image segmentation through dual-task consistency. In: *Proceedings of the AAAI Conference on Artificial Intelligence*, vol. 35, pp. 8801–8809 (2021)
- [38] Zhou, Y., Li, Z., Bai, S., Wang, C., Chen, X., Han, M., Fishman, E., Yuille, A.L.: Prior-aware neural network for partially-supervised multi-organ segmentation. In: *Proceedings of the IEEE/CVF International Conference on Computer Vision*, pp. 10672–10681 (2019)
- [39] Baid, U., Ghodasara, S., Mohan, S., Bilello, M., Calabrese, E., Colak, E., Farahani, K., Kalpathy-Cramer, J., Kitamura, F.C., Pati, S., *et al.*: The rsna-asnr-miccai brats 2021 benchmark on brain tumor segmentation and radiogenomic classification. *arXiv preprint arXiv:2107.02314* (2021)

---

**Algorithm 1** Staged Voxel-level Deep Reinforcement Learning Algorithm

---

**Require:** Segmentation model  $f_\theta$  with policy network  $\pi$  and value network  $V$ ; Let  $\theta_s$ ,  $\theta_v$ , and  $\theta_p$  denote the parameters of the segmentation model, value network, and policy, respectively; Training dataset  $\mathcal{D}$ ; batch size  $B$ ; max epochs  $T$ ; Learning rate  $\eta$ ; discount factor  $\gamma$ ; temperature  $\tau$ .

**Ensure:** Optimized model  $f_{\theta^*}$

```
1: Initialize model  $f_\theta$  and transition buffer  $\mathcal{B}$  stores experience tuples of the form
   ( $s, a, r, s'$ ).
2: for epoch  $t = 1$  to  $T$  do
3:   if  $t < t_{\text{Warmup}}$  then
4:     Compute  $\mathcal{L}_s = \ell_{\text{dice}}(f_\theta(x), y)$ 
5:     Update  $\theta \leftarrow \theta - \eta \nabla \mathcal{L}_s$ 
6:   end if
7:   if  $t_{\text{Warmup}} < t < t_{\text{Transition}}$  then
8:     for  $k = 1$  to  $K$  steps do
9:       Sample  $a \sim \pi(x; \tau)$  ▷ Policy with temperature
10:      Apply  $x' \leftarrow \text{Take Action}(x, a)$ 
11:      Store  $(x, a, r, x')$  in  $\mathcal{B}$ 
12:       $x \leftarrow x'$ 
13:    end for
14:    Compute  $R_t = r_t + \gamma R_{t+1}$  ▷ Discounted returns
15:     $\Delta\theta_v \leftarrow \nabla (R_t - V(x))^2$  ▷ Value loss
16:     $\Delta\theta_s \leftarrow \nabla \ell_{\text{loss}}(f_\theta(x), y)$  ▷ Segmentation loss
17:     $\theta \leftarrow \theta - \eta (\lambda \Delta\theta_v + (1 - \lambda) \Delta\theta_s)$ 
18:  else
19:    Initialize  $\tau = 0$ 
20:    for  $k = 1$  to  $K$  steps do
21:      Sample  $a \sim \pi(x; \tau)$ 
22:      Apply  $x' \leftarrow \text{apply\_medical\_effect}(x, a)$ 
23:      Store  $(x, a, r, x')$  in  $\mathcal{B}$ 
24:       $x \leftarrow x'$ 
25:    end for
26:    Compute  $R_t = r_t + \gamma R_{t+1}$ 
27:     $\Delta\theta_p \leftarrow -\mathbb{E}[\nabla \log \pi(a|x) A_t]$  ▷ policy gradient
28:     $\Delta\theta_v \leftarrow \nabla (R_t - V(x))^2$ 
29:     $\Delta\theta_s \leftarrow \nabla \ell(f_\theta(x), y)$ 
30:     $\theta \leftarrow \theta - \eta (\alpha \Delta\theta_p + \beta \Delta\theta_v + (1 - \alpha - \beta) \Delta\theta_s)$ 
31:  end if
32: end for
```

---